Current Opinion in Solid State and Materials Science 20 (2016) 247–256

Contents lists available at ScienceDirect

Current Opinion in Solid State and Materials Science

journal homepage: www.elsevier.com/locate/cossms

Grain boundary complexions and pseudopartial wetting

B.B. Straumal [a,b,c,*], A.A. Mazilkin [a,b], B. Baretzky [a]

[a] Karlsruher Institut für Technologie, Institut für Nanotechnologie, Hermann-von-Helmholtz-Platz 1, 76344 Eggenstein-Leopoldshafen, Germany
[b] Institute of Solid State Physics, Russian Academy of Sciences, Ac. Ossipyan str. 2, 142432 Chernogolovka, Russia
[c] National University of Science and Technology «MISIS», Leninsky prosp. 4, 119991 Moscow, Russia

ARTICLE INFO

Article history:
Received 25 November 2015
Revised 28 March 2016
Accepted 8 May 2016
Available online 17 May 2016

Keywords:
Grain boundary
Complexions
Pseudopartial wetting

ABSTRACT

The important class of grain boundary (GB) complexions includes the few nanometer thick layers having composition which strongly differs from that of the abutting grains. Such GB complexions are frequently called intergranular films (IGFs) and can be observed close to the lines of wetting, prewetting and premelting complexion transitions in the bulk phase diagrams. In the majority of systems, the direct transition between complete and partial GB wetting takes place (by changing temperature, pressure, etc.). However, in certain conditions the so-called pseudopartial (or pseudoincomplete, or frustrated complete) GB wetting appears in a phase diagram between complete and partial wetting. In case of pseudopartial GB wetting, the thin GB layer of a complexion (IGF or 2-D interfacial phase) can coexist with large droplets (or particles) of the wetting phase with a non-zero dihedral (contact) angle. Thus, such IGFs can be observed in the two-phase (or multiphase) fields of bulk phase diagrams, in the broad intervals of concentrations, temperature and/or pressure. The IGFs driven by the pseudopartial GB wetting can drastically modify the properties of polycrystals. In this review, we discuss this phenomenon for the technologically important Fe–Nd–B-based hard magnetic alloys, WC–Co cemented carbides and Al-based light alloys.

1. Introduction

The developments of last decade show that properties of fine-grained and nanograined materials are critically controlled by the behaviour of grain boundaries (GBs) and triple junctions (TJs) [1–4]. Moreover, the most advanced experimental methods like high-resolution electron microscopy (HREM) and atom probe microscopy allowed observing that GBs and TJs are frequently not atomically thin and smooth but contain the few nm thick layers or so-called intergranular films (IGFs) [3–21]. Such IGFs form the important class of grain boundary complexions [5,6,21] having composition which strongly differs from that of the abutting grains. These layers can appear in equilibrium, non-equilibrium (transient) or steady-state structures [4–20,22–31]. In the majority of cases such surface and GB complexions are intimately connected with GB wetting, prewetting and premelting equilibrium complexion transformations (for review see [5,6] and references therein). Such GB transformations were first predicted in seminal works of Cahn [32] and Ebner and Saam [33]. They analysed the transition between complete (CW, Fig. 1c, d, and g) and partial (PW, Fig. 1a, b, and g) wetting close to the critical point in a two-component phase diagram. However, most interestingly, from our point of view, is the phenomenon of the so-called pseudopartial (or pseudoincomplete, or frustrated complete [34]) GB wetting (Fig. 1e and f) marked as PPW in the generic phase diagram (Fig. 1g proposed in Ref. [35]) [36–39]. The pseudopartial GB wetting is intermediate between complete (Fig. 1d) and partial (Fig. 1b) GB wetting. PPW was first predicted by de Gennes [40]. De Gennes analysed the influence of the so-called Hamaker constant on wetting phenomena [40]. In case of pseudopartial GB wetting, thin GB layer of a second phase (i.e. IGF or complexion) can coexist with droplets (or particles) of a second phase with large non-zero contact (dihedral) angle (Fig. 1f). It means that such IGFs or GB complexions of high adsorption levels can be observed in the two-phase (or multiphase) fields of bulk phase diagrams (in addition to the single phase regions), i.e. in the broad ranges of concentrations, temperature and/or pressure. The IGFs can drastically modify the properties of polycrystals.

In this review we will demonstrate the presence of pseudopartial GB wetting for technologically important Fe–Nd–B-based hard magnetic alloys [41,42], WC–Co cemented carbides [39] and Al–Zn light alloys [37,38]. The IGFs of Nd-rich phase magnetically isolate the $Nd_2Fe_{14}B$ grains from each other and make Fe–Nd–B-based alloys the best known hard magnetic alloys with highest magnetic energy product *HB* (*B* being the flux density and *H* being the field

* Corresponding author at: Institute of Solid State Physics, Russian Academy of Sciences, Chernogolovka, Moscow District, 142432, Russia.
E-mail address: straumal@issp.ac.ru (B.B. Straumal).

http://dx.doi.org/10.1016/j.cossms.2016.05.006
1359-0286/

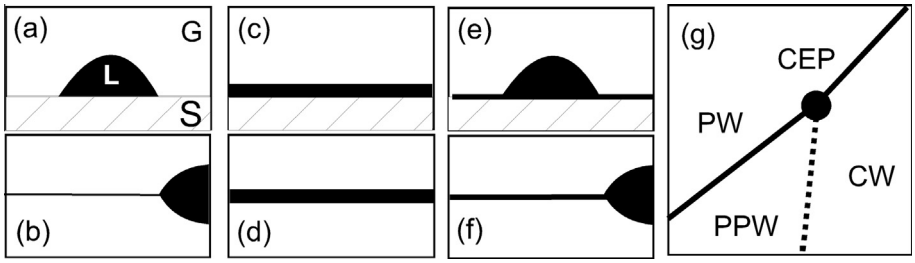

Fig. 1. The schemes for the wetting of free surfaces and GBs. (a) partial surface wetting, L – liquid phase, S – solid phase, G – gas phase; (b) partial GB wetting; (c) complete surface wetting; (d) complete GB wetting; (e) pseudopartial surface wetting; (f) pseudopartial GB wetting; (g) generic wetting phase diagram [33], PW – partial wetting, CW – complete wetting, PPW – pseudopartial wetting, CEP – critical end point, thick lines mark the discontinuous (first order) wetting transition, thin dotted line mark the continuous (second order) wetting transition.

strength) [43,44]. Thin IGFs of Co binder form the ductile skeleton between grains of hard tungsten carbide and ensure their unique combination of high hardness, wear-resistance, toughness and strength [39,45–47]. The 2–4 nm thin Zn-rich layers (complexions) between Al grains cause superductility of the ultrafine-grained Al–Zn alloys obtained by the high pressure torsion [26–28,48,49].

2. Definition of pseudopartial wetting

The pseudopartial (or pseudoincomplete, or frustrated complete) wetting, where the bulk phase of a fluid has a nonzero contact angle on top of a film of the same fluid, has been of interest in the scientific literature since the end of 1980s [34–40,50–53]. Let us consider a partially melted two- or multicomponent polycrystal between solidus temperature T_S and liquidus temperature T_L. Consider the droplet of a liquid phase on the surface of a solid phase or between two solid grains. Usually one distinguishes partial (incomplete) and complete wetting of surfaces or interfaces. In case of complete wetting the contact angle θ is zero. If the contact angle θ is between zero and 180° one speaks about partial or incomplete wetting [6]. We will use further this terminology though in some literature sources one speaks about partial wetting when the contact angle is between 90° and 180°. In these sources one uses "wetting" (meaning complete or perfect wetting) vs. "non-wetting" (including partial wetting, which is "non-wetting" thermodynamically) [6].

If a liquid droplet partially wets a solid surface (Fig. 1a) then $\sigma_{sg} - \sigma_{sl} = \sigma_{lg} \cos\theta$, where σ_{sg} is the free energy of solid/gas interface, σ_{sl} is the free energy of solid/liquid interface, σ_{lg} is that of liquid/-gas interface. If a liquid droplet partially wets the boundary between two solid grains (Fig. 1b), then $\sigma_{gb} = 2\,\sigma_{sl} \cos\theta$, where σ_{gb} is the free energy of a grain boundary. The free surface or GB which is not covered by the liquid droplets remains dry and contains only adsorbed atoms of a second component with coverage below one monolayer. In this case the GB can exist in the equilibrium contact with the liquid phase. If $\sigma_{sg} = \sigma_{lg} + \sigma_{sl}$ or $\sigma_{gb} = 2\,\sigma_{sl}$ complete wetting of free surface or grain boundary takes place and θ reaches zero (Fig. 1c and d) [54]. We have to underline here the subtle but important difference between "dry" interfaces and equilibrium interfaces [19,54,55]. In the criteria used above, the terms σ_{sg} and σ_{gb} actually refer to the so-called "dry" or "clean" surface or GB before wetting (without adsorption of the wetting phase) [19,54,55]. However, the wetted surface or GB is the new interface thermodynamically [54]. In the literature, there are two ways to differentiate this subtle, but important, difference. In the surface wetting community, one frequently use σ_{sv} (meaning the solid/vacuum interface) to denote that it is different from the equilibrium σ_{sg} (meaning the equilibrium solid/gas interface, which, at equilibrium, will be wetted so that $\sigma_{sg} = \sigma_{lg} + \sigma_{sl}$ [54]). This notation is difficult to be used for denoting "dry" or "clean" GBs, so other authors use symbols like σ^0_{gb} [19,55] to differentiate "dry" or "clean" GBs from the equilibrium GBs with equilibrium adsorption, disordering or wetting (here wetting means adsorption with infinite GB excess). Thus, in the case $\sigma_{sg} > \sigma_{lg} + \sigma_{sl}$ or $\sigma_{gb} > 2\,\sigma_{sl}$, the contact angle θ also remains zero, and liquid spreads over the free surface or between grains. In this case, a GB separating abutting grains is completely substituted by the liquid phase.

The transition from incomplete to complete (partial) GB wetting proceeds at a certain T_w if the energy of two solid-liquid interfaces $2\,\sigma_{SL}$ becomes lower than the GB energy $\sigma_{GB} > 2\,\sigma_{SL}$. Cahn [32] and Ebner and Saam [33] first showed that the (reversible) transition from incomplete to complete wetting can proceed with increasing temperature, and that it is a true surface phase (complexion) transformation. The GB wetting temperatures T_w, depend both on GB energy and solid-liquid interfacial energy which, in turn, depend on the crystallography of these interfaces [56–59]. The transition from incomplete to complete GB wetting starts at a certain minimum temperature T_{wmin}. T_{wmin} is determined by combination of maximum σ_{GB} and minimum σ_{SL}. The transition from incomplete to complete GB wetting finishes at a maximum temperature T_{wmax}. T_{wmax}, in turn, is determined by combination of minimum σ_{GB} and maximum σ_{SL}. The fraction of completely wetted GBs increases from 0 to 100% as the temperature increases from T_{wmin} to T_{wmax} [60–65]. As a result, the new tie-lines appear in the S + L area of a phase diagram at T_{wmin} and T_{wmax} [60–65].

In case of complete wetting (Fig. 1c and d), $\sigma_{sg} > \sigma_{lg} + \sigma_{sl}$ or $\sigma_{gb} > 2\,\sigma_{sl}$, contact angle θ is zero, and liquid spreads over the free surface or between grains. What happens, if the amount of liquid is small and surface (or GB) area is large? In this case the liquid spreads until the abutting solid grains or solid and gas begin to interact with each other through the liquid layer. The liquid forms a "pancake" with thickness e_s about 2–5 nm [11,66]:

$$e_s = (A/4\pi S)^{1/2}, \tag{1}$$

where $S = \sigma_{sg} - \sigma_{sl} - \sigma_{lg}$ is the spreading coefficient on a strictly "dry" solid and A is the Hamaker constant [40,66]. In case of complete wetting, $A > 0$ and $S > 0$ [40,66]. Such "pancake" (complexion) on the free surface or between two grains is formed by the deficit of a wetting phase. Such conditions can be found in the α + L two-phase area of a phase diagram, but in the narrow "temperature (pressure) - concentration" band very close to the solidus line.

In the majority of cases, the direct transition occurs from partial wetting into complete wetting, for example by increasing temperature [59,67,68] or decreasing pressure [69]. However, in some cases, the pseudopartial wetting (PPW in Fig. 1g) appears between partial and complete wetting. In this case the contact angle $\theta > 0$, the liquid droplet does not spread over the substrate, but the thin (few nm) precursor film exists around the droplet and separates substrate and gas (Fig. 1e). Such thin precursor film (complexion) is very similar to the liquid "pancake" which forms in case of

complete wetting and deficit of the liquid phase. This case is called pseudopartial wetting, it is possible when $A < 0$ and $S > 0$ [66]. In case of pseudopartial wetting the precursor exists simultaneously with liquid droplets. In case of complete wetting, conversely, the droplets disappear and form a "pancake".

The sequence of discontinuous PW ↔ PPW and continuous PPW ↔ CW has been observed for the first time in the alcanes/water mixture [70]. The critical end point (CEP in Fig. 1f) was observed in a mixture of pentane and hexane which was deposited on an aqueous solution of glucose [35]. The first direct measurement of the contact angle in the intermediate wetting state (pseudo-partial wetting) was performed in the sequential-wetting scenario of hexane on salt brine [70]. Later the formation of Pb, Bi and binary Pb–Bi precursors surrounding liquid or solidified droplets has been observed on the surface of solid copper [71].

3. Grain boundary IGFs (complexions) and pseudopartial wetting in the Fe–Nd–B-based magnets, WC–Co cemented carbides and Al-based light alloys

3.1. Fe–Nd–B-based permanent magnets

Nd–Fe–B-based alloys for permanent magnets were invented in 1980s. They remain up to now the best known hard magnetic alloys with highest magnetic energy product *HB* (*B* being the flux density and *H* being the field strength). In order to reach the optimum magnetic properties, the $Nd_2Fe_{14}B$ grains have to be isolated one from another by the layers of a non-ferromagnetic phase. In most cases it is the Nd-rich phase. The Nd-rich phase appears during the liquid-phase sintering as liquid layer between $Nd_2Fe_{14}B$ grains. It has been demonstrated rather early [43], that the thickness of these layers needed for effective magnetic isolation between $Nd_2Fe_{14}B$ grains is only few nanometers [44]. Such 2–5 nm thick layers (IGFs or complexions) in $Nd_2Fe_{14}B/Nd_2Fe_{14}B$ GBs were recently observed using HREM [72–74]. If the total amount of the Nd-rich phase is too high, it decreases the saturation magnetization of an alloy as a whole. Therefore, the amount of the Nd-rich phase has to be kept as low as possible, namely at the level which is minimally needed for the effective magnetic isolation between grains of the hard magnetic $Nd_2Fe_{14}B$ phase. It is the reason for the technological interest to the thin GB layers (IGFs or complexions) in the Nd–Fe–B-based alloys.

In [42] the Nd–Fe–B-based liquid-phase sintered alloy was purchased from the company Vacuumschmelze GmbH (Germany), it contained 66.5 wt% Fe, 22.1 wt% Nd, 9.4 wt% Dy, 1.0 wt% Co, 0.8 wt% B, 0.2 wt% Cu. Samples were sealed into evacuated silica ampoules and annealed at 900 °C for 2 h, and then quenched in water. Transmission electron microscopy (TEM, HRTEM, STEM, EDXS) studies were carried out on the TECNAI instrument. X-ray diffraction (XRD) data were obtained on a Siemens diffractometer (Co Kα radiation). TEM lamellas were prepared on the STRATA dual beam facility.

In Fig. 2a the STEM micrograph of a triple joint between three $Nd_2Fe_{14}B$ grains is shown. Chemical composition of these three grains measured by the EDXS in TEM corresponds to that of $Nd_2Fe_{14}B$ hard magnetic phase. Triple joint shown in Fig. 2a is filled by the Nd-rich phase. The Nd-rich phase was liquid during the liquid phase sintering and annealing at 900 °C [75–77]. Fig. 2d–f shows the Fe and Nd concentration profiles across all three $Nd_2Fe_{14}B/Nd_2Fe_{14}B$ GBs in the locations C, B and A (Fig. 2a), respectively. The first two profiles do not contain any Fe and/or Nd maxima or minima. It means that the respective GBs C and B remain "dry" and are not enriched (depleted) by the Fe and/or Nd. The GBs C and B have the non-zero contact angle with Nd-rich phase in the triple junction. In other words, the GBs C and B are incompletely (partially) wetted by the Nd-rich melt. This situation corresponds to the scheme shown in Fig. 1b.

The GB A is different. The concentration profile in Fig. 2f shows that GB A is enriched by Nd and depleted by Fe. The width of the Nd maximum and Fe minimum in Fig. 2f is about 5 nm. The uniformly thin light-grey layer of a Nd-rich phase is clearly visible also in GB A (Fig. 2a). Fig. 2b shows the conventional TEM micrograph of this GB and Fig. 2c contains the micrograph of the same GB with a thin layer of a Nd-rich phase. Both TEM and HREM also witness that the Nd-rich GB layer is uniformly thin and has a thickness of about 5 nm. The GB A, similar to the GBs C and B, also has the non-zero contact angle with Nd-rich phase in the triple junction. Since GB A is not "dry" and contains the thin Nd-rich layer, this situation corresponds to the scheme shown in Fig. 1f. In other words, the GB C is pseudo-incompletely (or pseudo-partially) wetted by the Nd-rich melt.

Therefore, the boundaries between grains of $Nd_2Fe_{14}B$ hard magnetic phase in the NdFeB-based permanent magnets can be pseudo-incompletely (or pseudo-partially) wetted by the Nd-rich melt [42]. Such GBs form the non-zero contact angle with the melt in the triple junctions and, simultaneously, contain the uniformly thin (about 5 nm) Nd-rich layer. Therefore, they are different from the completely wetted GBs (zero contact angle and non-uniform and thick Nd-rich layer with thickness above 100 nm), and incompletely wetted GBs (non-zero contact angle, no Nd-rich layer). The thin Nd-rich layers in the pseudo-incompletely (pseudo-partially) wetted $Nd_2Fe_{14}B/Nd_2Fe_{14}B$ GBs are most probably responsible for the excellent magnetic properties of the NdFeB-base permanent magnets. It is because these layers can ensure the magnetic isolation between the $Nd_2Fe_{14}B$ grains needed for the high coercivity.

3.2. WC–Co cemented carbides

WC–Co cemented carbides are metal-ceramic composites consisting of a ceramic phase, namely tungsten carbide, and a cobalt binder. They are broadly used in various industrial applications and almost in each household, for example, as masonry drill bits, due to their unique combination of high hardness, wear-resistance, toughness and strength. Since their discovery in Germany in the 1920s, WC–Co cemented carbides did not dramatically change. The main improvements were related to varying WC grain size, Co content and employing inhibitors of WC grain growth during liquid phase sintering [78,79]. The key to the exceptional properties of cemented carbides is the optimal combination of hardness and wear-resistance of WC grains, and toughness and ductility of the Co-based matrix. Also, the presence of a carbide skeleton of WC grains in the carbide microstructure appears to play a very important role for the unique combination of hardness and fracture toughness of cemented carbides. The skeleton can be designated as the "pseudo-skeleton", based on the fact that almost all the WC-WC grain boundaries are known to comprise very thin Co interlayers of the order of from nearly one atomic monolayer to several nanometers [45–47]. In this respect, the wetting of boundaries between WC grains by the Co melt during liquid phase sintering is the key issue. It is because pure WC/WC grain boundaries not comprising the Co interlayers should be quite brittle. It is well known that the wettability of WC by liquid Co examined by the method of a lying droplet is complete, and the wetting angle of a droplet of liquid Co on the surface of WC is equal to 0 at temperatures of 1400–1500 °C [80,81].

Nevertheless, the presence of the "pseudo-skeleton" of WC grains in the cemented carbide microstructure clearly indicates that WC/WC GBs are characterised by various contact angles with the cobalt-based binder and only very few angles are equal to 0° [39]. Therefore, there is a contradiction between the complete wetting of WC surface by the liquid Co droplets, on the one hand, and

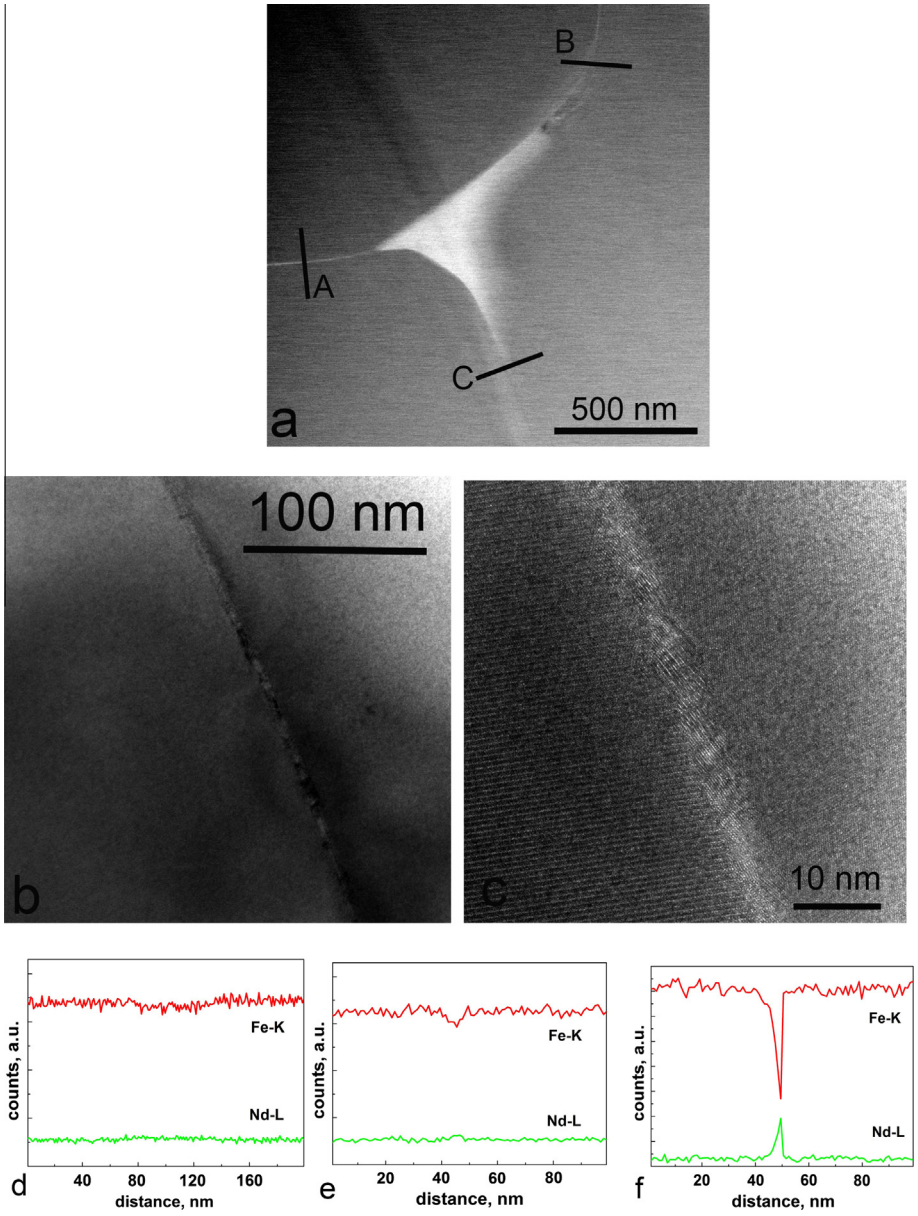

Fig. 2. (a) STEM micrograph of a triple joint between three $Nd_2Fe_{14}B$ grains filled by the Nd-rich phase. The positions of concentration profiles are shown (A, B and C). (b) Conventional TEM micrograph of a GB A containing the uniformly thin layer of a Nd-rich phase. (c) HREM micrograph of the same GB with a thin layer of a Nd-rich phase. (d–f) Fe and Nd concentration profiles in the locations C, B and A, respectively. Figure is reproduced from Ref. [42] with the permission of Springer.

the contact angles between WC/WC GBs and the Co binder different from 0 in the carbide microstructure, on the other hand. This contradiction was mentioned as early as in 1972 by Warren and Waldron [82]. It can be explained by the pseudopartial GB wetting in cemented carbides and existence of respective GB IGFs or complexions [39].

Ultra-coarse WC-Co cemented carbides were produced according to the procedure described in Ref. [83]. The WC powder (MAS 3000–5000, H.C. Starck) was milled with 10 wt% Co in an attritor-mill for 1 h in hexane with 2 wt% paraffin wax. Samples were pressed and liquid-phase sintered at 1380 °C for 75 min (45 min vacuum + 30 min HIP). The cross-sections were then investigated by means of optical microscopy and scanning electron microscopy (SEM). SEM investigations were carried out on a Tescan Vega TS5130 MM microscope equipped with the LINK energy-dispersive spectrometer produced by Oxford Instruments. Transmission electron microscopy (TEM, HRTEM, STEM, EDXS) studies were carried out on the TECNAI microscope.

Histogram indicating the share of WC/WC GBs having a certain contact angle with the Co-based binder shows that there are only very few contact angles equal to 0° ($\theta = 0°$) corresponding to the complete GB wetting [39]. Fig. 3a [39] shows the Z-contrast image obtained by HAADF STEM in the contact area between two WC grains (bright) and the grain of Co-based binder (dark, removed during the preparation of TEM sample). EDS profile of Co concentration across WC/WC GB shown in Fig. 3b demonstrates that this GB contains a thin Co-based layer of nearly 5–7 nm (white line in Fig. 3a). The position of respective line profile is shown in Fig. 3a. The spatial resolution of EDS is about 1–2 nm, the step between points is 1 nm. It means that a gradual composition profile in Fig. 3b is mainly due to the EDS spatial resolution. The contact (dihedral) angle of the WC/WC GB with Co grain (dark, removed during the preparation) is about 90° and, therefore, it is far away from zero. Therefore, the Co-rich thin layer (complexion) in WC/WC GB (Fig. 3b) is a typical example of pseudopartial GB wetting. To our minds, the phenomenon of PPW can explain the special

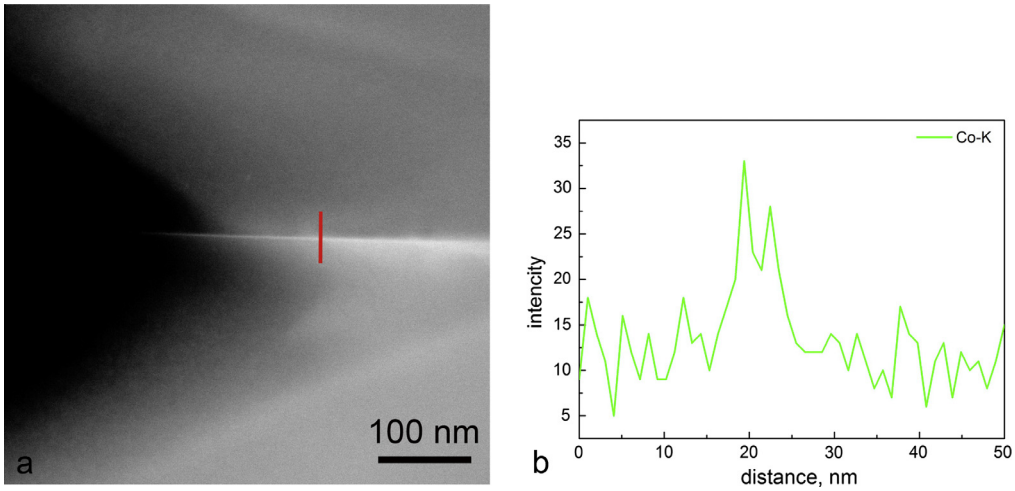

Fig. 3. (a) STEM HAADF image showing the contact area between two WC grains (bright) and the grain of Co-based binder (dark, removed by the preparation of TEM sample). WC/WC grain boundary contains the 5–7 nm thin layer of Co-rich phase (white). (b) EDS profile of Co concentration across WC/WC GB. The position of respective line profile is shown in (a). Figure is reproduced from Ref. [39] with the permission of Elsevier.

features of the cemented carbide microstructure and apparent contradiction between the fact of complete wetting of WC surface by a liquid Co droplet and non-zero contact angles between the WC-WC GBs and Co binder.

3.3. Al-based light alloys

In first two cases of Nd–Fe–B-based hard magnetic alloys and WC-Co cemented carbides, the IGFs or complexions were formed in GBs during the liquid phase sintering, i.e. in the contact with liquid phase. In case of the Al–Zn light alloys the liquid phase was absent, and the formation of Zn-rich IGFs or complexions in the Al/Al GBs was ensured by the accelerated mass transfer driven by the so-called severe plastic deformation (SPD). SPD is a family of methods allowing to producing the extremely high strains in a material without its failure (because the material is deformed in a confined space) [84]. A very high density of lattice defects appearing during SPD drives various bulk phase transformations [85,86]. In case of Al–Zn alloys SPD (exactly speaking – high pressure torsion, HPT) drives not only bulk phase transition (decomposition of supersaturated solid solution of Zn in Al) bust also the GB transformation, namely the formation of Zn-rich IGFs or complexions in Al/Al GBs [39].

HPT (5 GPa, 300 K, 5 torsions, 1 rpm) was applied to the Al – 30 wt% Zn polycrystals made of high-purity components [39]. The analytical TEM has been performed with a probe-corrected ARM200F JEOL microscope operated at 200 kV. High Angle Annular Dark Field (HAADF) images were recorded in the scanning mode (STEM) using a probe size of 0.2 nm with a convergence angle of 34 mrad and collection angles in the range of 80–300 mrad. To quantify the local Zn concentrations, energy-dispersive X-ray spectroscopy (EDS) was performed using a JEOL JED2300 detector. Similar to Refs. [87,88], the supersaturated (Al) solid solution almost completely decomposed. The mean Al grain size decreased from 500 μm before deformation to 400 nm after HPT.

The HPT-treated Al–Zn alloys contain some (about 20%) Al/Al GBs with a thin uniform Zn-enriched layer contacting with Zn grains and having non-zero contact angle. Such case is shown in Fig. 4. The contact area of a Zn grain (left bottom corner) and an Al/Al GB (aligned from left bottom to right top) is clearly exhibited (Fig. 4a). The contact (dihedral) angle of the (solid) Zn grain with the Al/Al GB is about 94°.

It is important to underline, that the question of GB wetting becomes far from trivial if the wetting (second) phase is not liquid but solid. Recently, the GB wetting by a second solid phase has been investigated in detail both experimentally [89–93] and theoretically [6,94,95]. Most important difference is that if the wetting phase is solid, the anisotropy of interfacial energies leads to the torque terms in Young equation which cannot be neglected [6,94,95]. However, the long anneals (like in experiments [89–93]) can equilibrate the microstructure, and in this case one can speak about equilibrium GB contact (dihedral) angles. We have to underline, that in case of HPT the microstructure reaches not the equilibrium state (like after long anneals [89–93]) but the steady-state. It is reached in the Al-based alloys after 0.5–1 rotation of anvils and further remains unchanged [87]. One can even speak about so-called equifinal state [96–98]. The *equi*final state of an open system is reached in the steady-state and does not depend on the starting state of the system [99]. It is similar to that as *equi*librium state of a closed system is reached after long equilibrating annealing and does not depend on the starting state as well.

The respective Al/Al GB clearly appears on the image as a bright line, indicating a local Zn enrichment. This feature was confirmed by the EDS line scan analysis performed across the Al/Al boundary (Fig. 4b). The maximum Zn concentration across the Al/Al boundary is 15 ± 0.5 at.%, and large gradients are exhibited (over 4 nm on each side of the interface, also confirmed by the plot of the HAADF signal across the GB in Fig. 4b). Part of this gradient might be attributed to a misalignment of the Al/Al GB under the electron beam. However, one should note that a 2 nm wide plateau is clearly exhibited on the profile, indicating that the Al/Al GB is not wetted completely by a pure Zn layer. Moreover, the thickness of a Zn-rich GB layer is very uniform along all visible GBs. The micrograph obtained with HREM (Fig. 4b) shows the intermediate layer between Al grains with higher magnification. Its thickness is about 2 nm. If one analyses numerous GBs after HPT, one can observe, contrary to the long annealed samples [64], not only Al/Al GBs completely and partially wetted by the solid Zn phase, but also numerous GBs with $\theta > 0$ and thin Zn-enriched layer. The contact angles for these GBs vary between $\theta = 80$ and 160°, and TEM data show that they are not symmetric. The increase of θ from 80 and 160° correlates with thickness decrease of Zn-enriched GB layers from 10 to 2 nm. The PW GBs do not have any visible Zn-enrichment and have contact angles between $\theta = 120$ and 180°.

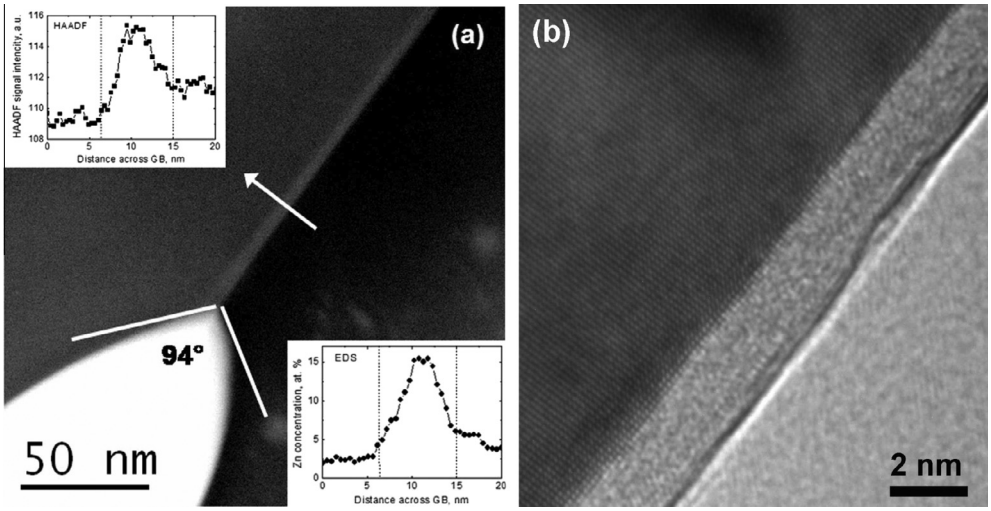

Fig. 4. (a) Z-contrast image obtained by HAADF STEM showing a Zn grain (bright) in the bottom left corner and an Al/Al grain boundary (aligned from left bottom to right top) covered by a uniform Zn rich layer in the Al – 30 wt% Zn alloy after HPT (5 GPa, 5 rot. 1 rpm). The contact angle of the Zn grain with the Al/Al GB is 94°. Left inset: HAADF signal intensity across the Al/Al GB showing that the apparent thickness of the Zn rich layer is about 8 nm (the arrow in (a) indicated the location of the profile) Right inset: Zn concentration gradient across the Al/Al GB at the same place, estimated by EDS. (b) HRTEM image showing a featureless wetting layer along an Al/Al GB. Figure is reproduced from Ref. [37] with the permission of Elsevier.

The Zn-enriched GB layer in Fig. 4b looks structureless (or amorphous), like the GB complexions in sintered oxides [7,10,11,13,14]. However, one has to discuss this feature very cautiously. It might be not the equilibrium but equifinal and, therefore, controlled by HPT process. One needs here more experimental evidence, for example by studying the Al–Zn alloys with various Zn concentrations.

Therefore, the experimental evidence is found in [37] that the pseudopartial wetting exists even in the case when the second (wetting) phase is not liquid but solid. This phenomenon takes place in the Al–Zn system, where the discontinuous GB wetting transition occurs in the (Al)+L two-phase area of the phase diagram and it changes to the continuous one in the (Zn)+L area [67]. The PPW was observed not after conventional annealing and subsequent quenching, but after the HPT in the steady-state stage. The PPW Zn-enriched GB films (complexions) can also explain the unusual superductility of ultra-fine grained Al–Zn alloys after HPT [26,27,48,49].

4. Link between GB complexions and pseudopartial GB wetting

Close to the bulk solidus line the prewetting (premelting) IGFs or complexions exist in GBs. They are observed between GB and bulk solidus lines in the bulk phase diagram. Such IGFs are structurally similar to the thin GB films formed in case of complete GB wetting and deficit of a wetting phase (c.f. Section 2). For example, the prewetting/premelting films have been directly observed by HRTEM for two metallic systems W–Ni and Mo–Ni where the complexions appear to be disordered "quasi-liquid" interfacial films of ~1 nm thick in HRTEM of quenched specimens [100,101]. The IGFs GB and bulk solidus lines lead to the high GB diffusivity [103–105], increased GB mobility [106–108] or GB brittleness [58,102,109]. The first (temperature) derivative of GB energy breaks at the GB solidus line. It means that the formation of prewetting/premelting IGFs or complexions is the phase transition of first order [58]. The measurements on the Cu–Bi samples showed that the electrical conductivity abruptly increased when the network of Bi-rich layers isolating the copper grains one from another had broken [109]. The extreme superplasticity of ultra-fine-grained Al–Zn–Mg alloys (with elongation to failure up to 2500%) in the narrow temperature interval just below the bulk solidus [110–115] is also driven by the formation of liquid-like IGFs or complexions between GB and bulk solidus lines [116,117]. In Al–Zn alloys, the IGFs or complexions between GB and bulk solidus were observed by HREM [116,117], they even give visible input in the melting peak in the calorimetric curves (Fig. 5) [23]. In turn, the calorimetric curves (Fig. 5) permitted us to construct the GB solidus line in the Al–Zn phase diagram (Fig. 6) [23].

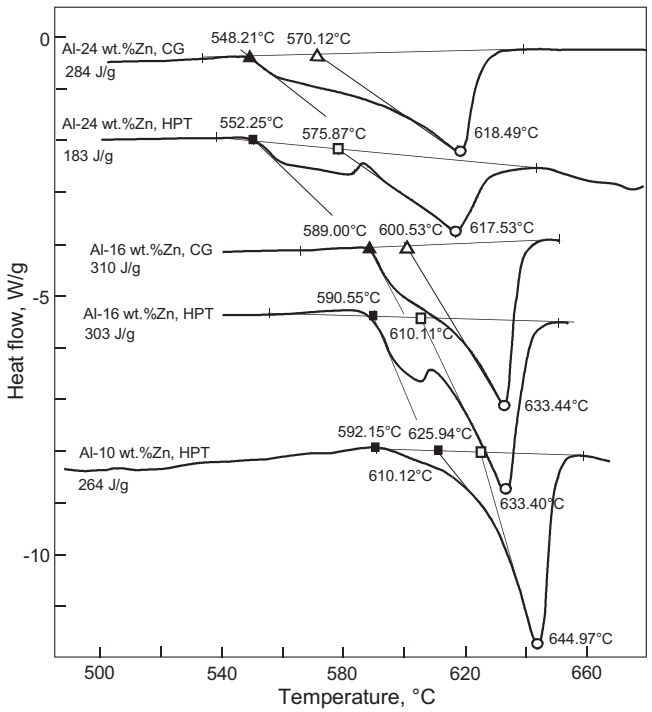

Fig. 5. Temperature dependence of heat flow (DSC curves) for the Al–Zn samples. ○ – liquidus temperature, △ – bulk solidus for coarse-grained (CG) alloys, □ – bulk solidus for fine-grained (HPT) alloys, ▲ – GB solidus for coarse-grained (CG) alloys, ■ – GB solidus for fine-grained (HPT) alloys. Figure is reproduced from Ref. [23] with the permission of Elsevier.

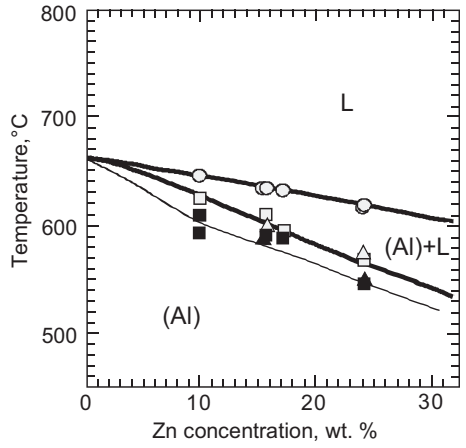

Fig. 6. Part of the Al–Zn phase diagram. Thick lines mark the bulk liquidus and solidus [16]. Thin line mark GB solidus. Experimental points are taken from Fig. 4: ○ – liquidus temperature, △ – bulk solidus for coarse-grained (CG) alloys, □ – bulk solidus for fine-grained (HPT) alloys, ▲ – GB solidus for coarse-grained (CG) alloys, ■ – GB solidus for fine-grained (HPT) alloys. Figure is reproduced from Ref. [23] with the permission of Elsevier.

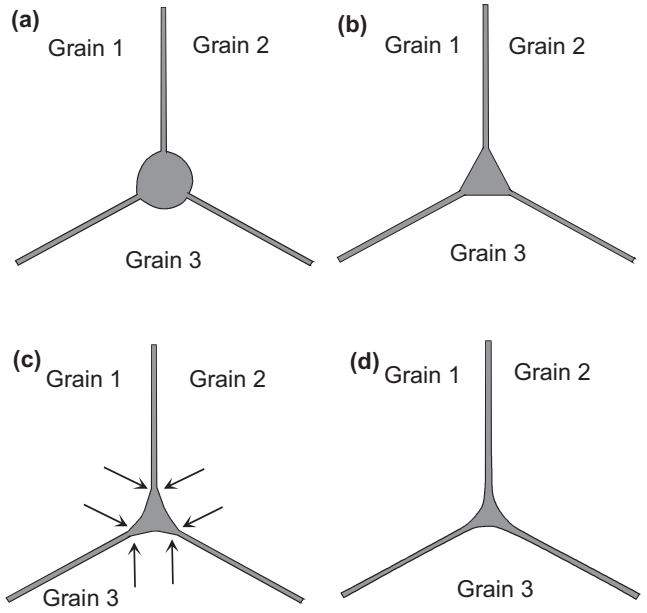

Fig. 7. Different configurations of liquid phase in the GB triple junction and thin quasi-liquid thin layers in the GB. (a) Pseudopartial GB wetting, $\theta > 60°$. (b) Pseudopartial GB wetting, $\theta = 60°$. (c) Pseudopartial GB wetting, $\theta < 60°$. The contact points between liquid phase in TJ and quasi-liquid layers in the GB are shown by arrows. (d) Complete GB wetting, $\theta = 0°$. Figure is reproduced from Ref. [132] with the permission of Trans Tech Publications.

The nature of quasi-liquid (or liquid-like) complexions between bulk solidus line and GB solidus line (like those observed in W–Ni [100], Mo–Ni [101], Al–Zn–Mg [110–115], Al–Zn [23,116,117], Fe–Si–Zn [104], Al–Ga [106] and Cu–Bi [102,106,118,119] alloys) is very interesting. On the one hand, simple thermodynamic reasons permit one to expect that the composition of these thin GB layers should correspond to the point at the bulk liquidus line. On the other hand, it is hard to imagine that the layer having thickness of few nm possess the properties close to those of "true" (i.e. bulk) liquid phase. The main experimental problem is that it is hardly possible to investigate the structure of these layers *in situ*, in other words, at high temperature between bulk solidus line and GB solidus line. Quenching to the room temperature strongly changes the structure of these GB complexions. Similar to the quenching of bulk liquids, the GB complexions in ceramics (like ZnO [120–126] or Si_3N_4 [10–14]) remain amorphous after cooling and those in metallic alloys (like Cu–Bi [102,106], Ni–Bi [10], W–Ni [100], Mo–Ni [101] or Al–Zn [116]) crystallize. Only kinetic properties of these liquid-like complexions (or controlled by those GB layers) can be measured really *in situ*, namely at high temperature. The examples are GB diffusivity [103–105,118], GB mobility [106–108], GB brittleness [58,102,109] or superplasticity controlled by the GB sliding [110–115].

If one observes the thin GB layers of a constant thickness (multilayer complexions), it is not easy to distinguish, whether one has the case of (1) prewetting/prewetting in the one-phase area of a bulk phase diagram; (2) thin GB "pancake" due to the deficit of wetting phase or (3) pseudopartial GB wetting by a liquid or solid phase. The big problem is that most frequently the wetting phase (either bulk liquid or second solid phase) can be found only in the TJ "pockets". The pseudopartial wetting can be clearly identified only if the GB contact (dihedral) angle $\theta \geqslant 60°$ and the solid/liquid interface is convex (Fig. 7a and b). If the contact angle is low, $\theta < 60°$, and the solid/liquid interface is concave (Fig. 7c and d), the difference becomes very tiny. If the solid/liquid interface has a discontinuity (two tangentials) between TJ pocket and GB layer (Fig. 7c), the pseudopartial wetting clearly takes place. If the solid/liquid interface is continuous between TJ pocket and GB layer and one can draw only one tangential (Fig. 7d), then the complete wetting with the deficit of wetting phase takes place.

Thin IGFs (bilayer or multilayer complexions) were experimentally observed also in many other systems [10,11,13,14,20,120–126]. Frequently these cases are quite promising from the point of view of possible pseudopartial wetting. For example, it has been found recently that in Ni–Bi alloys, the average contact (dihedral) angle is >40° (i.e. nonzero) while the GBs are covered continuously by a bilayer interfacial phase (complexion) [20]. Also, the equilibrium-thickness intergranular films that are widely observed in Si_3N_4 and many other liquid-phase sintered ceramics above the bulk solidus lines also coexist with non-wetting liquid phases (at the sintering temperatures) [11].

The good example is also zinc oxide. ZnO is mainly used for manufacturing of varistors. Varistors exhibit highly non-linear current–voltage characteristics with a high resistivity below a threshold electric field, becoming conductive when this field is exceeded, enabling them to be used in current over-surge protection circuits. The model usually proposed to account for the electrical properties of ZnO-based varistors is constituted on the basis of a bricklayer. ZnO-based varistors are approximated as a stacking of good conducting grains separated by grain boundaries, which support back-to-back double Schottky barriers [120,121]. Polycrystalline zinc oxide contains small amounts of dopants, mainly bismuth oxide. After liquid-phase sintering, such material consists of ZnO grains separated by the Bi_2O_3-rich GB layers. Interfaces between the ZnO grains control the non-linear current-voltage characteristics. The intergranular phase originates from the liquid-phase sintering. The sintering conditions alter the performances of ZnO varistors [120]. An increase in the sintering temperature results usually in a lowering in the nonlinearity of the current–voltage curve. Bhushan et al. pointed out that an increase in the sintering temperature would lower the Schottky barrier height [122] and Wong mentioned that the volatilization of Bi_2O_3 during the sintering would bring a loss in the non-ohmic property of the varistors [123]. In ZnO–Bi_2O_3 samples studied in Ref. [124] can be clearly seen that the amorphous Bi-rich thin GB layer has the non-zero contact angle with the Bi_2O_3 phase in TJs. This situation corresponds to scheme in Fig. 7c and not to that in Fig. 7d. In other words, the *pseudopartial GB wetting* has been observed in Ref.

[124]. Most probably, the pseudopartial GB wetting ZnO–Bi_2O_3 system is observed not in all GBs and not in all conditions. For example, the TJs in Refs. [125,126] clearly correspond to the scheme Fig. 7d (complete wetting, $\theta = 0°$). These are also many examples showing that pseudopartial GB wetting can be found in many systems.

5. Conclusions and outlook

The IGFs (bilayer and multilayer complexions) were frequently observed in grain boundaries close to the lines of wetting, prewetting and premelting transitions in the bulk phase diagram. Previously only direct transition between complete and partial GB wetting has been experimentally observed. However, in certain conditions the indirect transition between complete and partial wetting takes place through the intermediate state, namely the pseudopartial (or pseudoincomplete, or frustrated complete) GB wetting. In case of pseudopartial GB wetting, a thin GB layer of a second phase (complexion) coexists with large droplets (particles) of the wetting phase and the GB contact angle remains high (non-zero). In this review we analysed first experimental observations of such IGFs or complexions in case of pseudopartial GB wetting in the technologically important Fe–Nd–B-based hard magnetic alloys, WC–Co cemented carbides and Al-based light alloys.

In a classic case, prewetting complexions only exist in the one-phase area of a phase diagram (when the wetting phase is unstable in the bulk). On the contrary, the GB complexions connected with pseudopartial GB wetting can be observed in a broader range of phase fields in binary and multicomponent phase diagrams, including two- and multiphase regions, coexisting with the pseudopartial-wetting phases that form non-zero contact (dihedral) contacts where they meet the pseudopartial-wetting complexions. Therefore, such IGFs or GB complexions can be used as a fine instrument for the so-called grain boundary engineering (term first introduced by Tadao Watanabe [127]). As we saw in this review, the IGFs can improve the magnetic properties (Fe–Nd–B-based hard magnetic alloys), fracture toughness and strength (WC–Co cemented carbides) or formability (Al-based light alloys).

The experimental search for the IGFs and pseudopartial GB wetting in the technologically important alloys should be based on the (rather cheap) SEM screening of GB wetting in polycrystals combined with (expensive and sophisticated) aberration-corrected HREM studies of individual GBs. Even more complicated (but not less important) should be the experimental investigations of the linear (or tubular) few nm thick enriched layers in the GB triple junctions and in dislocation cores. The wetting conditions for such linear defects are different from those for GBs [128,129], they were expected to serve as channels for the quick formation of GB films [130], and recently they were indeed observed in experiments [4,131].

Acknowledgements

The work was performed under the partial financial support of Russian Foundation for Basic Research (Grants 14-42-03621, 15-03-01127 and 15-53-06008), The Ministry of Education and Science of the Russian Federation in the Framework of Increase Competitiveness Program of MISiS, Israeli Ministry of Science, Technology and Space, and Karlsruhe Nano Micro Facility operated by the Karlsruhe Institute of Technology.

References

[1] B.B. Straumal, A.A. Mazilkin, S.G. Protasova, A.A. Myatiev, P.B. Straumal, G. Schütz, P.A. van Aken, E. Goering, B. Baretzky, Grain-boundary induced high T_c-ferromagnetism in pure and doped nanocrystalline ZnO, Phys. Rev. B 79 (2009) 205206.
[2] B. Zhao, G. Gottstein, L.S. Shvindlerman, Triple junction effects in solids, Acta Mater. 59 (2011) 3510–3518.
[3] J.G. Dash, H. Fu, J.S. Wettlaufer, The premelting of ice and its environmental consequences, Rep. Prog. Phys. 58 (1995) 115–167.
[4] M. Kuzmina, M. Herbig, D. Ponge, S. Sandlöbes, D. Raabe, Linear complexions: confined chemical and structural states at dislocations, Science 349 (2015) 1080–1083.
[5] P.R. Cantwell, T. Ming, S.J. Dillon, J. Luo, G.S. Rohrer, M.P. Harmer, Grain boundary complexions, Acta Mater. 62 (2014) 1–48.
[6] W.D. Kaplan, D. Chatain, P. Wynblatt, W.C. Carter, A review of wetting versus adsorption, complexions, and related phenomena: the Rosetta stone of wetting, J. Mater. Sci. 48 (2013) 5681–5717.
[7] P. Bueno, J. Varela, E. Longo, SnO_2, ZnO and related polycrystalline compound semiconductors, an overview and review on the voltage-dependent resistance (non-ohmic) feature, J. Eur. Ceram. Soc. 28 (2008) 505–529.
[8] J. Luo, Y.M. Chiang, R.M. Cannon, Nanometer-thick surficial films in oxides as a case of prewetting, Langmuir 21 (2005) 7358–7365.
[9] J. Luo, M. Tang, R.M. Cannon, W.C. Carter, Y.M. Chiang, Pressure-balance and diffuse-interface models for surficial amorphous films, Mater. Sci. Eng. A 422 (2006) 19–28.
[10] D.R. Clarke, On the equilibrium thickness of intergranular glass phases in ceramic materials, J. Am. Ceram. Soc. 70 (1987) 15–22.
[11] J. Luo, Stabilization of nanoscale quasi-liquid interfacial films in inorganic materials: a review and critical assessment, Crit. Rev. Solid State Mater. Sci. 32 (2007) 67–109.
[12] J. Luo, Y.M. Chiang, Wetting and prewetting on ceramic surfaces, Ann. Rev. Mater. Res. 38 (2008) 227–249.
[13] A. Subramaniam, C. Koch, R.M. Cannon, M. Rühle, Intergranular glassy films: an overview, Mater. Sci. Eng. A 422 (2006) 3–18.
[14] I. Maclaren, Imaging and thickness measurement of amorphous intergranular films using TEM, Ultramicroscopy 99 (2004) 103–113.
[15] S.J. Dillon, M. Tang, W. Craig Carter, M.P. Harmer, Complexion: a new concept for kinetic engineering in materials science, Acta Mater. 55 (2007) 6208–6218.
[16] M.P. Harmer, Interfacial kinetic engineering: how far have we come since Kingery's inaugural Sosman address?, J Am. Ceram. Soc. 93 (2010) 301–317.
[17] S.G. Protasova, B.B. Straumal, A.A. Mazilkin, S.V. Stakhanova, P.B. Straumal, B. Baretzky, Increase of Fe solubility in ZnO induced by the grain boundary adsorption, J. Mater. Sci. 49 (2014) 4490–4498.
[18] Th. Tietze, P. Audehm, Y.C. Chen, G. Schütz, B.B. Straumal, S.G. Protasova, A.A. Mazilkin, P.B. Straumal, Th. Prokscha, H. Luetkens, Z. Salman, A. Suter, B. Baretzky, K. Fink, W. Wenzel, D. Danilov, E. Goering, Interfacial dominated ferromagnetism in nanograined ZnO: a μSR and DFT study, Sci. Rep. 5 (2015) 8871.
[19] N. Zhou, J. Luo, Developing grain boundary diagrams for multicomponent alloys, Acta Mater. 91 (2015) 202–216.
[20] J. Luo, H. Cheng, K.M. Asl, C.J. Kiely, P. Martin, M.P. Harmer, The role of a bilayer interfacial phase on liquid metal embrittlement, Science 333 (2011) 1730.
[21] M. Tang, W. Craig Carter, R.M. Cannon, Diffuse interface model for structural transitions of grain boundaries, Phys. Rev. B 73 (2006) 024102.
[22] B.B. Straumal, A.A. Mazilkin, S.G. Protasova, S.V. Stakhanova, P.B. Straumal, M. F. Bulatov, G. Schütz, Th. Tietze, E. Goering, B. Baretzky, Grain boundaries as a source of ferromagnetism and increased solubility of Ni in nanograined ZnO, Rev. Adv. Mater. Sci. 41 (2015) 61–71.
[23] B. Straumal, R. Valiev, O. Kogtenkova, P. Zieba, T. Czeppe, E. Bielanska, M. Faryna, Thermal evolution and grain boundary phase transformations in severe deformed nanograined Al–Zn alloys, Acta Mater. 56 (2008) 6123–6131.
[24] O.A. Kogtenkova, B.B. Straumal, S.G. Protasova, A.S. Gornakova, P. Zięba, T. Czeppe, Effect of the wetting of grain boundaries on the formation of a solid solution in the Al–Zn system, JETP Lett. 96 (2012) 380–384.
[25] R.Z. Valiev, M.Yu Murashkin, B.B. Straumal, Enhanced ductility in ultrafine-grained Al alloys produced by SPD techniques, Mater. Sci. Forum 633–634 (2009) 321–332.
[26] R.Z. Valiev, M.Y. Murashkin, A. Kilmametov, B.B. Straumal, N.Q. Chinh, T.G. Langdon, Unusual super-ductility at room temperature in an ultrafine-grained aluminum alloy, J. Mater. Sci. 45 (2010) 4718–4724.
[27] N.Q. Chinh, T. Csanádi, J. Gubicza, R.Z. Valiev, B.B. Straumal, T.G. Langdon, The effect of grain-boundary sliding and strain rate sensitivity on the ductility of ultrafine-grained materials, Mater. Sci. Forum 667–669 (2011) 677–682.
[28] N.Q. Chinh, T. Csanádi, T. Győri, R.Z. Valiev, B.B. Straumal, M. Kawasaki, T.G. Langdon, Strain rate sensitivity studies in an ultrafine-grained Al–30 wt% Zn alloy using micro- and nanoindentation, Mater. Sci. Eng. A 543 (2012) 117–120.
[29] W.E. Frazier, G.S. Rohrer, A.D. Rollett, Abnormal grain growth in the Potts model incorporating grain boundary complexion transitions that increase the mobility of individual boundaries, Acta Mater. 96 (2015) 390–398.
[30] W. Rheinheimer, M.J. Hoffmann, Non-Arrhenius behavior of grain growth in strontium titanate: new evidence for a structural transition of grain boundaries, Scripta Mater. 101 (2015) 68–71.
[31] A.K. Lawrence, A. Kundu, M.P. Harmer, C. Compson, J. Atria, M. Spreij, J. Am. Ceram. Soc. 98 (2015) 1347–1355.
[32] J.W. Cahn, Critical point wetting, J. Chem. Phys. 66 (1977) 3667–3676.

[33] C. Ebner, W.F. Saam, New phase-transition phenomena in thin argon films, Phys. Rev. Lett. 38 (1977) 1486–1489.
[34] D. Bonn, J. Eggers, J. Indekeu, J. Meunier, E. Rolley, Wetting and spreading, Rev. Mod. Phys. 81 (739–80) (2009) 5.
[35] S. Rafaï, D. Bonn, E. Bertrand, J. Meunier, Long-range critical wetting, observation of a critical end point, Phys. Rev. Lett. 92 (2004) 245701.
[36] J. Moon, P. Wynblatt, S. Garoff, R. Suter, Diffusion kinetics of Bi and Pb–Bi monolayer precursing films on Cu(1 1 1), Surf. Sci. 559 (2004) 149–157.
[37] B.B. Straumal, X. Sauvage, B. Baretzky, A.A. Mazilkin, R.Z. Valiev, Grain boundary films in Al–Zn alloys after high pressure torsion, Scripta Mater. 70 (2014) 59–62.
[38] B.B. Straumal, A.A. Mazilkin, X. Sauvage, R.Z. Valiev, A.B. Straumal, A.M. Gusak, Pseudopartial wetting of grain boundaries in severely deformed Al–Zn alloys, Russ. J. Non-Ferrous Met. 56 (2015) 44–51.
[39] B.B. Straumal, I. Konyashin, B. Ries, A.B. Straumal, A.A. Mazilkin, K.I. Kolesnikova, A.M. Gusak, B. Baretzky, Pseudopartial wetting of WC/WC grain boundaries in cemented carbides, Mater. Lett. 147 (2015) 105–108.
[40] F. Brochard-Wyart, J.M. di Meglio, D. Quéré, P.-G. De Gennes, Spreading of nonvolatile liquids in a continuum picture, Langmuir 7 (1991) 335–338.
[41] B.B. Straumal, A.A. Mazilkin, S.G. Protasova, A.M. Gusak, M.F. Bulatov, A.B. Straumal, B. Baretzky, Grain boundary phenomena in NdFeB-based hard magnetic alloys, Rev. Adv. Mater. Sci. 38 (2014) 17–28.
[42] B.B. Straumal, A.A. Mazilkin, S.G. Protasova, G. Schütz, A.B. Straumal, B. Baretzky, Observation of pseudopartial grain boundary wetting in the NdFeB-based alloy, J. Mater. Eng. Perform. 25 (2016). DOI:10.1007/s11665-015-1872-8.
[43] T. Schrell, J. Fidler, H. Kronmüller, Remanence and coercivity in isotropic nanocrystalline permanent magnets, Phys. Rev. B 49 (1994) 6100–6110.
[44] D. Goll, M. Seeger, H. Kronmüller, Magnetic and microstructural properties of nanocrystalline exchange coupled PrFeB permanent magnets, J. Magn. Magn. Mater. 185 (1998) 49–60.
[45] N.K. Sharma, I.D. Ward, H.L. Fraser, W.S. Williams, STEM analysis of grain boundaries in cemented carbides, J. Am. Ceram. Soc. 63 (1980) 194–196.
[46] A. Henjered, M. Hellsing, H.O. Andren, H. Norden, Quantitative microanalysis of carbide-carbide interfaces in WC-Co cemented carbides, J. Mater. Sci. Technol. 2 (1986) 847–855.
[47] J. Weidow, H.-O. Andrén, Grain and phase boundary segregation in WC–Co with TiC, ZrC, NbC or TaC additions, Int. J. Refr. Met. Hard Mater. 29 (2011) 38–43.
[48] N.Q. Chinh, R.Z. Valiev, X. Sauvage, G. Varga, K. Havancsák, M. Kawasaki, B.B. Straumal, T.G. Langdon, Grain boundary phenomena in an ultrafine-grained Al–Zn alloy with improved mechanical behavior for micro-devices, Adv. Eng. Mater. 16 (2014) 1000–1009.
[49] X. Sauvage, MYu Murashkin, B.B. Straumal, E. Bobruk, R.Z. Valiev, Ultrafine grained structures resulting from SPD-induced phase transformation in Al-Zn alloys, Adv. Eng. Mater. 17 (2015). DOI: 10.1002/adem.201500151.
[50] K.D. Humfeld, S. Garoff, P. Wynblatt, Analysis of pseudopartial and partial wetting of various substrates by lead, Langmuir 20 (2004) 2726–2729.
[51] N. Churaev, Wetting films and wetting, Rev. Phys. Appl. 23 (1988) 975–987.
[52] A. Sharma, Equilibrium contact angles and film thicknesses in the apolar and polar systems: role of intermolecular interactions in coexistence of drops with thin films, Langmuir 9 (1993) 3580–3586.
[53] Y. Solomentsev, L.R. White, Microscopic drop profiles and the origins of line tension, J. Colloid Interface Sci. 218 (1999) 122–136.
[54] P.G. de Gennes, Wetting: statics and dynamics, Rev. Mod. Phys. 57 (1985) 827–863.
[55] J. Luo, Developing interfacial phase diagrams for applications in activated sintering and beyond: current status and future directions, J. Am. Ceram. Soc. 95 (2012) 2358–2371.
[56] B.B. Straumal, L.M. Klinger, L.S. Shvindlerman, The effect of crystallographic parameters of interphase boundaries on their surface tension and parameters of the boundary diffusion, Acta Metall. 32 (1984) 1355–1364.
[57] B.B. Straumal, S.A. Polyakov, E.J. Mittemeijer, Temperature influence on the faceting of Σ3 and Σ9 grain boundaries in Cu, Acta Mater. 54 (2006) 167–172.
[58] J. Schölhammer, B. Baretzky, W. Gust, E. Mittemeijer, B. Straumal, Grain boundary grooving as an indicator of grain boundary phase transformations, Interface Sci. 9 (2001) 43–53.
[59] B. Straumal, T. Muschik, W. Gust, B. Predel, The wetting transition in high and low energy grain boundaries in the Cu(In) system, Acta Metal. Mater. 40 (1992) 939–945.
[60] B. Straumal, G. López, W. Gust, E. Mittemeijer, Effect of the grain boundary phase transitions on the superplasticity in the Al–Zn system, in: M.J. Zehetbauer, R.Z. Valiev (Eds.), Nanomaterials by Severe Plastic Deformation. Fundamentals – Processing – Applications, Wiley VCH, Weinheim, Germany, 2004, pp. 642–647.
[61] C.-H. Yeh, L.-S. Chang, B.B. Straumal, The study on the solidus line in Sn-rich region of Sn–In phase diagram, J. Phase Equilbria Diff. 30 (2009) 254–257.
[62] B.B. Straumal, G. López, E.J. Mittemeijer, W. Gust, A.P. Zhilyaev, Grain boundary phase transitions in the Al–Mg system and their influence on the high-strain rate superplasticity, Def. Diff. Forum 216–217 (2003) 307–312.
[63] V. Murashov, B. Straumal, P. Protsenko, Grain boundary wetting in Zn bicrystals by a Sn-based melt, Def. Diff. Forum 249 (2006) 235–238.
[64] C.-H. Yeh, L.-S. Chang, B.B. Straumal, The grain boundary wetting in the Sn–25 at.% In alloys, Def. Diff. Forum 258–260 (2006) 491–496.
[65] B. Straumal, D. Molodov, W. Gust, Wetting transition on the grain boundaries in Al contacting with Sn-rich melt, Interface Sci. 3 (1995) 127–132.
[66] F. Brochard-Wyart, J.M. di Meglio, D. Quéré, P.G. de Gennes, Spreading of nonvolatile liquids in a continuum picture, Langmuir 7 (1991) 335–338.
[67] B.B. Straumal, A.S. Gornakova, O.A. Kogtenkova, S.G. Protasova, V.G. Sursaeva, B. Baretzky, Continuous and discontinuous grain boundary wetting in the Zn–Al system, Phys. Rev. B 78 (2008) 054202.
[68] B.B. Straumal, P. Zieba, W. Gust, Grain boundary phase transitions and phase diagrams, Int. J. Inorg. Mater. 3 (2001) 1113–1115.
[69] B. Straumal, E. Rabkin, W. Lojkowski, W. Gust, L.S. Shvindlerman, Pressure influence on the grain boundary wetting phase transition in Fe–Si alloys, Acta Mater. 45 (1997) 1931–1940.
[70] E. Bertrand, H. Dobbs, D. Broseta, J. Indekeu, D. Bonn, J. Meunier, First-order and critical wetting of alkanes on water, Phys. Rev. Lett. 85 (2000) 1282–1285.
[71] J. Moon, S. Garoff, P. Wynblatt, R. Suter, Pseudopartial wetting and precursor film growth in immiscible metal systems, Langmuir 20 (2004) 402–408.
[72] H. Sepehri-Amin, T. Ohkubo, K. Hono, Grain boundary structure and chemistry of Dy-diffusion processed Nd-Fe-B sintered magnets, J. Appl. Phys. 107 (2010) 09A745.
[73] N. Oono, M. Sagawa, R. Kasada, H. Matsui, A. Kimura, Microstructural evaluation of Dy-Ni-Al grain-boundary-diffusion (GBD) treatment on sintered Nd-Fe-B magnet, Mater. Sci. Forum 654 (2010) 2919–2922.
[74] T.H. Kim, S.R. Lee, S. Namkumg, T.S. Jang, A study on the Nd-rich phase evolution in the Nd-Fe-B sintered magnet and its mechanism during post-sintering annealing, J. Alloys Comp. 537 (2012) 261–268.
[75] Y. Matsuura, Y. Hirosawa, H. Yamamoto, S. Fujimura, M. Sagawa, K. Osamura, Phase diagram of the Nd-Fe-B ternary system, Jap. J. Appl. Phys. Part 2 – Lett. 24 (1985). L635-7.
[76] G. Schneider, E.-T. Henig, G. Petzow, H.H. Stadelmaier, Phase relations in the system Fe-Nd-B, Zt Metallkunde 77 (1986) 755–761.
[77] K.G. Knoch, B. Reinsch, G. Petzow, $Nd_2Fe_{14}B$ – its region of primary solidification, Zt Metallkunde 85 (1994) 350–353.
[78] A. Bose, A perspective on the earliest commercial PM metal-ceramic composite: cemented tungsten carbide, Int. J. Powder Metall. 47 (2) (2011) 31–50.
[79] H. Kolaska, The dawn of the hardmetal age, Powder Met. Int. 24 (1992) 311–314.
[80] J. Gurland, J.T. Norton, Role of the binder phase in cemented tungsten carbide-cobalt alloys, J. Metals 4 (1952) 1051–1056.
[81] L. Ramqvist, Hot pressing of metallic carbides, Powder Met. 9 (1966) 26–33.
[82] R. Warren, M.B. Waldron, Microstructural development during liquid-phase sintering of cemented carbides. 1. Wettability and grain contact, Powder Met. 30 (1972) 166–180.
[83] I. Konyashin, F. Schäfer, R. Cooper, J. Mayer, T. Weirich, Novel ultra-coarse hardmetal grades with reinforced binder for mining and construction, Int. J. Refract. Met. Hard Mater. 23 (2005) 225–232.
[84] R.Z. Valiev, R.K. Islamgaliev, I.V. Alexandrov, Bulk nanostructured materials from severe plastic deformation, Prog. Mater. Sci. 45 (2000) 103–189.
[85] B.B. Straumal, A.A. Mazilkin, B. Baretzky, E. Rabkin, R.Z. Valiev, Accelerated diffusion and phase transformations in Co–Cu alloys driven by the severe plastic deformation, Mater. Trans. 53 (2012) 63–71.
[86] B. Straumal, A. Korneva, P. Zięba, Phase transitions in metallic alloys driven by the high pressure torsion, Arch. Civil Mech. Eng. 14 (2014) 242–249.
[87] A.A. Mazilkin, B.B. Straumal, M.V. Borodachenkova, R.Z. Valiev, O.A. Kogtenkova, B. Baretzky, Gradual softening of Al–Zn alloys during high pressure torsion, Mater. Lett. 84 (2012) 63–65.
[88] B.B. Straumal, B. Baretzky, A.A. Mazilkin, F. Phillipp, O.A. Kogtenkova, M.N. Volkov, R.Z. Valiev, Formation of nanograined structure and decomposition of supersaturated solid solution during high pressure torsion of Al–Zn and Al–Mg, Acta Mater. 52 (2004) 4469–4478.
[89] S.G. Protasova, O.A. Kogtenkova, B.B. Straumal, P. Zięba, B. Baretzky, Inversed solid-phase grain boundary wetting in the Al–Zn system, J. Mater. Sci. 46 (2011) 4349–4353.
[90] G.A. López, E.J. Mittemeijer, B.B. Straumal, Grain boundary wetting by a solid phase; microstructural development in a Zn–5 wt% Al alloy, Acta Mater. 52 (2004) 4537–4545.
[91] B.B. Straumal, A.S. Gornakova, Y.O. Kucheev, B. Baretzky, A.N. Nekrasov, Grain boundary wetting by a second solid phase in the Zr–Nb alloys, J. Mater. Eng. Perform. 21 (2012) 721–724.
[92] B.B. Straumal, A.S. Gornakova, S.I. Prokofjev, N.S. Afonikova, B. Baretzky, A.N. Nekrasov, K.I. Kolesnikova, Continuous and discontinuous αTi layers between grains of β(Ti, Co) phase, J. Mater. Eng. Perform. 23 (2014) 1580–1584.
[93] B.B. Straumal, O.A. Kogtenkova, K.I. Kolesnikova, A.B. Straumal, M.F. Bulatov, A.N. Nekrasov, Reversible "wetting" of grain boundaries by the second solid phase in the Cu–In system, JETP Lett. 100 (2014) 535–539.
[94] P. Wynblatt, D. Chatain, Solid-state wetting transitions at grain boundaries, Mater. Sci. Eng. A 495 (2008) 119–125.
[95] P. Wynblatt, D. Chatain, Y. Pang, Some aspects of the anisotropy of grain boundary segregation and wetting, J. Mater. Sci. 41 (2006) 7760–7768.
[96] B.B. Straumal, A.A. Mazilkin, B. Baretzky, E. Rabkin, R.Z. Valiev, Accelerated diffusion and phase transformations in Co–Cu alloys driven by the severe plastic deformation, Mater. Trans. 53 (2012) 63–71.
[97] B.B. Straumal, A.R. Kilmametov, Yu.O. Kucheev, L. Kurmanaeva, Yu Ivanisenko, B. Baretzky, A. Korneva, P. Zięba, D.A. Molodov, Phase transitions during high pressure torsion of Cu–Co alloys, Mater. Lett. 118 (2014) 111–114.
[98] B.B. Straumal, A.R. Kilmametov, Yu Ivanisenko, A.A. Mazilkin, O.A. Kogtenkova, L. Kurmanaeva, A. Korneva, P. Zięba, B. Baretzky, Phase

transitions induced by severe plastic deformation: steady-state and equifinality, Int. J. Mater. Res. (formerly Z Metallkd) (2015) 106–164.
[99] L. von Bertalanffy, Problems of general system theory, Human Biol. 23 (1951) 302–312.
[100] J. Luo, V.K. Gupta, D.H. Yoon, H.M. Meyer III, Segregation-induced grain boundary premelting in nickel-doped tungsten, Appl. Phys. Lett. 87 (2005) 231902.
[101] X. Shi, J. Luo, Grain boundary wetting and prewetting in Ni-doped Mo, Appl. Phys. Lett. 94 (2009) 251908.
[102] A. Kundu, K.M. Asl, J. Luo, M.P. Harmer, Identification of a bilayer grain boundary complexion in Bi-doped Cu, Scripta Mater. 68 (2013) 146–149.
[103] B. Straumal, W. Gust, D. Molodov, Wetting transition on the grain boundaries in Al contacting with Sn-rich melt, Interface Sci. 3 (1995) 127–132.
[104] B.B. Straumal, O.I. Noskovich, V.N. Semenov, L.S. Shvindlerman, W. Gust, B. Predel, Premelting transition on 38°⟨1 0 0⟩ tilt grain boundaries in (Fe–10 at.% Si)–Zn alloys, Acta Metall. Mater. 40 (1992) 795–801.
[105] M.M. Moghadam, J.M. Rickman, M.P. Harmer, H.M. Chan, The role of boundary variability in polycrystalline grain-boundary diffusion, J. Appl. Phys. 117 (2016) 045311.
[106] D.A. Molodov, U. Czubayko, G. Gottstein, L.S. Shvindlerman, B.B. Straumal, W. Gust, Acceleration of grain boundary motion in Al by small additions of Ga, Phil. Mag. Lett. 72 (1995) 361–368.
[107] A. Tewari, F. Nabiei, S.C. Parker, M. Cantoni, M. Stuer, P. Bowen, C. Hébert, Toward knowledge-based grain-boundary engineering of transparent alumina combining advanced TEM and atomistic modelling, J. Am. Ceram. Soc. 98 (2015) 1959–1964.
[108] Y. Zu, G. Chen, X. Fu, K. Luo, C. Wang, S. Song, W. Zhou, Effects of liquid phases on densification of TiO_2-doped Al_2O_3-ZrO_2 composite ceramics, Ceram. Int. 40 (2014) 3989–3993.
[109] B. Straumal, N.E. Sluchanko, W. Gust, Influence of the grain boundary phase transitions on the properties of Cu–Bi polycrystals, Def. Diff. Forum 188–190 (2001) 185–194.
[110] K. Higashi, T.G. Nieh, M. Mabuchi, J. Wadsworth, Effect of liquid phases on the tensile elongation of superplastic aluminum alloys and composites, Scripta Metall Mater. 32 (1995) 1079–1084.
[111] Y. Takayama, T. Tozawa, H. Kato, Superplasticity and thickness of liquid phase in the vicinity of solidus temperature in a 7475 aluminum alloy, Acta Mater. 47 (1999) 1263–1270.
[112] M. Mabuchi, K. Higashi, Y. Okada, S. Tanimura, T. Imai, K. Kubo, Superplastic behavior at high strain rates in a particulate Si_3N_4/6061 aluminum composite, Scripta Metall. 25 (1991) 2003–2006.
[113] K. Higashi, Y. Okada, T. Mukai, S. Tanimura, Positive exponent strain-rate superplasticity in mechanically alloyed aluminum IN9021, Scripta Metall. 25 (1991) 2053–2057.
[114] H. Iwasaki, T. Mori, M. Mabuchi, K. Higashi, Shear deformation behavior of Al-5% Mg in a semi-solid state, Acta Mater. 46 (1998) 6351–6360.
[115] B. Baudelet, M.C. Dang, F. Bordeaux, Mechanical behaviour of an aluminium alloy with fusible grain boundaries, Scripta Metall. Mater. 26 (1992) 573–578.
[116] B.B. Straumal, A.A. Mazilkin, O.A. Kogtenkova, S.G. Protasova, B. Baretzky, Grain boundary phase observed in Al–5 at.% Zn alloy by using HREM, Phil. Mag. Lett. 87 (2007) 423–430.
[117] B. Straumal, O. Kogtenkova, S. Protasova, A. Mazilkin, P. Zieba, T. Czeppe, J. Wojewoda-Budka, M. Faryna, Wetting and premelting of triple junctions and grain boundaries in the Al–Zn alloys, Mater. Sci. Eng. A 495 (2008) 126–131.
[118] S.V. Divinski, M. Lohmann, Chr Herzig, B. Straumal, B. Baretzky, W. Gust, Grain boundary melting phase transition in the Cu–Bi system, Phys. Rev. B 71 (2005) 104104.
[119] L.-S. Chang, E. Rabkin, B.B. Straumal, S. Hoffmann, B. Baretzky, W. Gust, Grain boundary segregation in the Cu–Bi system, Def. Diff. Forum 156 (1998) 135–146.
[120] T.K. Gupta, Application of zinc oxide varistors, J. Am. Ceram. Soc. 73 (1990) 1817–1840.
[121] F. Greuter, G. Blatter, Electrical properties of grain boundaries in polycrystalline compound semiconductors, Semicond. Sci. Technol. 5 (1990) 111–137.
[122] B. Bhushan, S.C. Kashyap, K.L. Chopra, Electrical and dielectric behaviour of a zinc oxide composite, J. Appl. Phys. 52 (1981) 2932–2936.
[123] J. Wong, Sintering and varistor characteristics of ZnO–Bi_2O_3 ceramics, J. Appl. Phys. 51 (1980) 4453–4459.
[124] W. Onreabroy, N. Sirikulrat, A.P. Brown, C. Hammond, S.J. Milne, Properties and intergranular phase analysis of a ZnO–CoO–Bi_2O_3 varistor, Solid State Ionics 177 (2006) 411–420.
[125] J. Gambino, D. Kingery, G. Pike, L. Levinson, H.J. Philipp, Effect of heat treatments on the wetting behavior of bismuth-rich intergranular phases in ZnO–Bi–Co varistors, J. Am. Ceram. Soc. 72 (1989) 642–645.
[126] J.R. Lee, Y.M. Chiang, Bi segregation at ZnO grain boundaries in equilibrium with Bi_2O_3–ZnO liquid, Solid State Ionics 75 (1995) 79–88.
[127] T. Watanabe, Key issues of grain boundary engineering for superplasticity, Mater. Sci. Forum 243 (1997) 21–30.
[128] B.B. Straumal, O. Kogtenkova, P. Zięba, Wetting transition of grain boundary triple junctions, Acta Mater. 56 (2008) 925–933.
[129] B.B. Straumal, B.S. Bokstein, A.B. Straumal, A.L. Petelin, First observation of a wetting transition in low-angle grain boundaries, JETP Lett. 88 (2008) 537–542.
[130] L.S. Chang, E. Rabkin, B.B. Straumal, B. Baretzky, W. Gust, The kinetics of grain boundary segregation of Bi in polycrystalline Cu, Mater. Sci. Forum 294 (296) (1999) 585–588.
[131] Y. Zhang, J. Luo, Observation of an unusual case of triple-line instability, Scripta Mater. 88 (2014) 45–48.
[132] B.B. Straumal, A.O. Rodin, A.E. Shotanov, A.B. Straumal, O.A. Kogtenkova, B. Baretzky, Pseudopartial grain boundary wetting: key to the thin intergranular layers, Def. Diff. Forum 333 (2013) 175–192.